

Article

The Activation of Mg Powder Promoted by Chloride and Activation Mechanism

Xiaoxuan Wang¹, Xiaoyan Guo¹, Lixiang Zhu¹, Shuo Wang^{1,*}, Meishuai Zou^{1,*} , Xiaodong Li¹, Xiaodong Zhang¹ and Tinglu Song² 

¹ School of Materials Science and Engineering, Beijing Institute of Technology, Beijing 100081, China; 18434360254@163.com (X.W.); gxy@bit.edu.cn (X.G.); 3220201235@bit.edu.cn (L.Z.); bitlxd@bit.edu.cn (X.L.); 17854264182@163.com (X.Z.)

² Experimental Center of Advanced Materials School of Materials Science & Engineering, Beijing Institute of Technology, Beijing 100081, China; song@bit.edu.cn

* Correspondence: wangshuo@bit.edu.cn (S.W.); zoums@bit.edu.cn (M.Z.)

Abstract: Magnesium has bright market prospects such as generating thrust for under water engines and hydrogen production. However, the passive oxide film on the surface of magnesium powder prevents the further reaction of magnesium with water at room temperature. In this paper, highly active magnesium-based materials were prepared via ball milling pure Mg with different chlorides (NiCl₂, CoCl₂, CuCl₂, FeCl₃). The activity of the as obtained powder was analyzed through Scanning Electron Microscopy (SEM), Energy dispersive X-ray spectroscopy (EDS), X-ray photoelectron spectroscopy (XPS), synchrotron X-ray tomography, Extended X-ray Absorption Fine Structure (EXAFS), etc. Among the various compositions, the Mg-6%CoCl₂ composite exhibited the best hydrogen production performance with a hydrogen generation volume of 423 mL/(0.5 g) and a conversion yield of 96.6%. The related activation mechanism was thoroughly studied, showing that the addition of chloride during ball milling can effectively break the continuity of oxide films on Mg surfaces and introduces a large number of micro defects. In addition, the EXAFS and tomography data verified that metallic cobalt was generated during the ball milling process, subsequently forming a Mg-Co micro glance cell, and the Cl⁻ in the system accelerates the corrosion of Mg. The active mechanism can be verified as synergistic effects of micro glance cell and as-generated surface microcracks.

Keywords: hydrogen production; magnesium powder activation; ball-milling; activation mechanism



Citation: Wang, X.; Guo, X.; Zhu, L.; Wang, S.; Zou, M.; Li, X.; Zhang, X.; Song, T. The Activation of Mg Powder Promoted by Chloride and Activation Mechanism. *Metals* **2021**, *11*, 1435. <https://doi.org/10.3390/met11091435>

Academic Editors: Jean-Louis Bobet and Mieczyslaw Jurczyk

Received: 13 August 2021
Accepted: 7 September 2021
Published: 10 September 2021

Publisher's Note: MDPI stays neutral with regard to jurisdictional claims in published maps and institutional affiliations.



Copyright: © 2021 by the authors. Licensee MDPI, Basel, Switzerland. This article is an open access article distributed under the terms and conditions of the Creative Commons Attribution (CC BY) license (<https://creativecommons.org/licenses/by/4.0/>).

1. Introduction

As a promising new energy source [1–3], magnesium-based materials with unique physical and chemical properties, exhibit high mass and volume energy density [4,5]. The abundant resources of magnesium in the earth (contents in crust and seawater are 2.4% and 0.13%, respectively) and low cost make it a promising candidate material for energy storage and energy conversion [6,7]. Magnesium has been employed in various applications. For instance, the burning of Mg in CO₂ showed high specific impulse performance [8–10], and the realization of high-efficiency powder ignition will determine the future application prospects of the engine [10]. Magnesium could react easily with water with high reaction speed and efficiency [11–13]. Interestingly, magnesium could achieve eco-friendly hydrolysis reaction with high purity hydrogen and nano-size Mg(OH)₂. However, once the hydrolysis reaction begins, a dense oxide film will generate on the surface of the magnesium, which would highly reduce the activity of magnesium powder [13–16]. To solve this problem, the development of novel material systems and multiple modification processes have been reported. The modification of magnesium-based materials, as well as the optimization of the hydrolysis process, has received much attention [17,18]. Current research on the activation of Mg mainly focuses on ball-milling modification. Grosjean et al. [19,20] found that the specific surface area of Mg powder decreased linearly along

with the increase of milling time, and correspondingly, the hydrolysis conversion rate increased from 9% to 26%. Huang et al. [21] mixed Mo and its compounds with Mg via ball milling, and found that Mg-10 wt% MoS₂ exhibited excellent hydrogen production efficiency by hydrolysis in seawater. The excellent catalytic effect was mainly attributed to the synergistic effect introduced by the addition of catalyst. On one hand, the specific surface area of Mg enhanced the mechanical crushing effect during the ball milling process. On the other hand, the Mg could form a galvanic in the seawater medium, which promotes the corrosion of Mg. Huang et al. [22] investigated the activity of Mg powder with Co₃O₄ addition during ball milling, which can produce Mg powders with smaller size and higher specific surface area. Furthermore, the Co₃O₄ accelerated reaction rates of Mg powder compared to pure Mg milled powders. Zou et al. [23] prepared highly reactive Mg-Al-based hydro-reactive materials using high-energy ball milling. The Mg-Al hydro-reactive materials had excellent hydrolysis performance and could react completely with seawater in a short time, which showed the feasibility of its utilization for green energy production. Matsuzaki et al. [24] studied the hydrogen production performance of Mg chips generated via the hydrolysis reaction in seawater by machining. A notable improvement in hydrogen formation production was observed after ball milling and the hydrolysis reaction rate can be enhanced by the presence of NaCl in water. The addition of Ni during ball milling showed little impact in the hydrolysis reaction within non-conductive media. Grosjean et al. [20] found a significant increase of the H₂ production by milling Mg sample with chloride ions for 30 min. They explained that the ball milling process would induce defects and accentuation of the pitting corrosion by Cl⁻. Kravchenko et al. [25] investigated the oxidation processes of Mg, Mg alloys with Ni, Co, Cu powder mixtures and ball milling alloy. Nearly stoichiometric amounts of hydrogen in respect to Mg can be obtained at production rates of up to 640 mL · g⁻¹ × min⁻¹ by oxidation of Mg-Co alloy or mechanically processed Mg-Co powder (“mechanical alloy”) in aqueous solutions of Na or K chlorides. Activator metals are not oxidized during this reaction. They assumed that Mg oxidation is the result of the electrochemical corrosion.

Besides the studies of Mg-metal activated composites and the reaction of Mg with chloride solutions, chloride salts were also proven to be effective in activating the hydrolysis of Mg in neutral water. Liu et al. [26] found that the 6 h-milled Mg-3mol% AlCl₃ exhibited excellent performance with a hydrogen yield of 93.86% and IHGR (initial hydrogen generation rate) of 455.9 mL min⁻¹(g Mg)⁻¹ within 1 h. Wang et al. [27] investigated the effect of Co or Ni and anions on Mg-H₂O reaction. Hydrogen was rapidly generated after adding Mg to an aqueous CoCl₂ solution due to the synergistic reaction of the pitting of Cl⁻ ions, the micro galvanic cells and the active Co or Ni formed by oxidization/reduction reaction. The results from Sun et al. [28] indicated that the activated Mg-CoCl₂ composites are very promising materials for hydrogen generation. The hydrolysis reaction of the Mg-6% CoCl₂ composite initiated immediately when immersed in pure water (50 °C).

The above studies show that chloride is effective in promoting the hydrolysis reaction of ball milling Mg. However, no detailed mechanism was revealed. In this work, we firstly studied the activity of ball-milled magnesium powder containing different chloride salts (6% NiCl₂, 6% CoCl₂, 6% CuCl₂, 6% FeCl₃). We then studied the inner morphology of ball milling Mg-6%CoCl₂ composite using synchrotron X-ray tomography and the valence state of cobalt through EXAFS. The synergistic effects of ball milling, micro-galvanic corrosion, and modification effect of Cl⁻ are attributed to the activation of Mg.

2. Experimental

2.1. Material Preparation

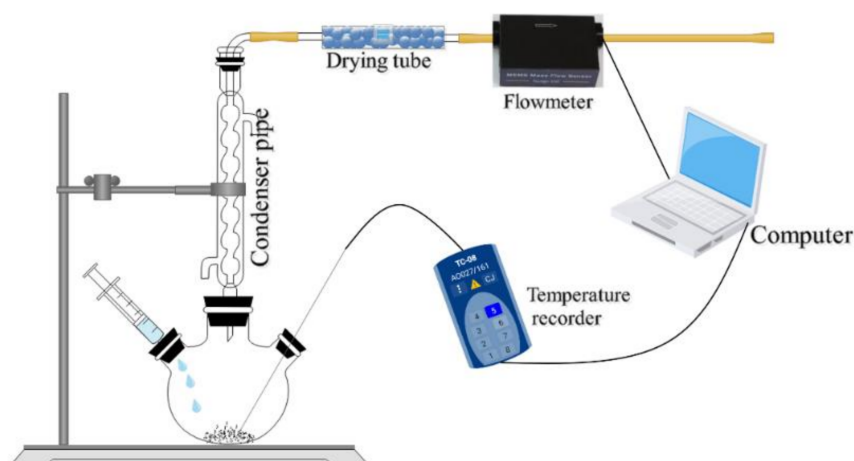
Magnesium powder (60–300 mesh, 99 wt.% purity), NiCl₂, CoCl₂, CuCl₂, and FeCl₃ (AR ≥ 99.5% purity) are the raw materials, the chloride content of ball milling is 6 percent of the mass fraction of Mg [28]. The milling process parameters are provided in Table 1. Masses of raw materials and water are 0.5 g and 10 g, with water to fuel ratio of 20:1.

Table 1. Ball milling parameters.

| Ball Milling | Parameters |
|--------------------------|----------------------------|
| Milling balls | Steel ball; diameter: 5 mm |
| Ball milling speed | 500 r/min |
| Ball milling atmosphere | Argon |
| Ball milling time | 3 h |
| Ball/material mass ratio | 40:1 |

2.2. Hydrolysis Experiment

The hydrolysis reaction was conducted at room temperature and under atmospheric pressure. As shown in Figure 1, the hydrogen production reaction was performed in a 100 mL three-necked flask, one neck for water addition, one neck for hydrogen outlet, and one neck for temperature measurement. The hydrogen generated flowed through a condenser pipe and drying tube to remove water vapor before passing through the gas mass flow sensor (MEMS-FS4008). The gas mass flow sensor was connected to a computer to record the instantaneous rate of gas and cumulative flow. The hydrogen production performance of each formulation was repeated at least 3 times.

**Figure 1.** Schematic of the experimental installation for measuring hydrogen.

2.3. Characterization Tests

The samples were analyzed by powder X-ray diffraction (XRD) using an X'Pert PRO MPD diffract meter (PANalytical, Almelo, Netherlands) with Cu K α radiation, the diffraction angle was selected from 2 to 90°. The sample morphologies were observed by FE-SEM S4800 (Hitachi Instruments Equipment, Tokyo, Japan) scanning electron microscopy (SEM) and the corresponding elemental mapping of the sample was obtained by energy-dispersive spectroscopy (EDS). The samples' binding energies were analyzed by powder X-ray photoelectron spectroscopy (XPS) using PHI QUANTERA-II SXM equipment (Ulvacphi Corporation, Kanagawa, Japan). The temperature change during the reaction was tested by a K-type thermocouple and recorded using a thermal recorder connecting to the computer. Tafel curve passed the test of 660E electrochemical platform. The Co K-edge XAFS and nano tomography measurements were performed at the beamline 4B9A and 4W1A-X of the Beijing Synchrotron Radiation Facility (BSRF) at the Institute of High Energy Physics (IHEP), Chinese Academy of Sciences (CAS).

3. Results

3.1. Characterization of Active Mg

All the raw materials show strong crystalline Mg peaks such as the XRD patterns shown in Figure 2. The Mg peaks of pure Mg/Mg-chloride structures after ball milling

and the Mg standard card are almost constant, only showing a difference in peak intensity. It shows that the crystal forms of Mg in the raw materials after ball milling are all the same, and the crystallinity of different crystal forms of Mg has changed after adding different chlorides.

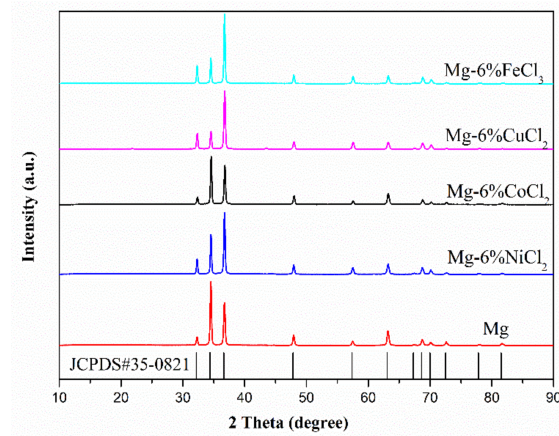


Figure 2. XRD patterns of Mg and Mg-chloride composites after ball-milling.

Figure 3 shows the SEM image of unmilled Mg, ball-milled Mg powder and the Mg-chlorides. All the spherical powders changed into flakes after ball milling. More structural defects were observed on the particles' surface after ball milling with chloride. This indicates that the oxide surface of the pure Mg powder can be effectively broken during the ball-milling process by adding chloride, exposing more reactive sites for the contact reaction between Mg and water.

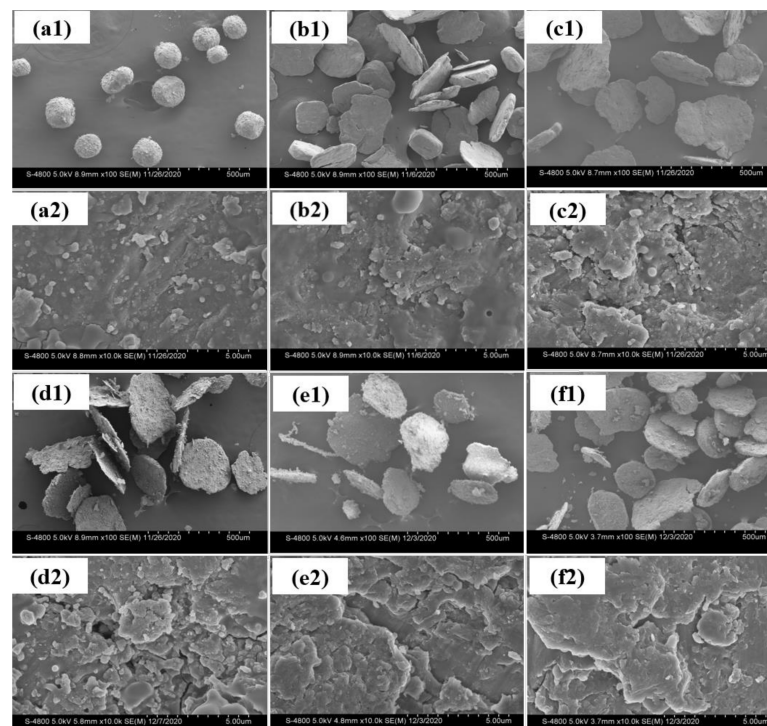


Figure 3. SEM images of unmilled Mg, ball-milled Mg and Mg-chlorides composites: (a1) unmilled Mg powder, (b1) ball-milled pure Mg, (c1) Mg-6wt.%NiCl₂, (d1) Mg-6wt.%CoCl₂, (e1) Mg-6wt.%CuCl₂, (f1) Mg-6wt.%FeCl₃. (a2–f2) are the corresponding amplified images.

XPS spectra were performed to investigate the electronic environment of Mg in different composites. The Mg element exists in two forms of pure Mg and MgO from the XPS spectra shown in Figure 4. The binding energy of elemental Mg is about 49.91 eV for ball-milled pure Mg. The MgO peak has a large area which indicates the existence of a large amount of oxidation on the surface. However, after adding chloride during ball milling, the binding energies of Mg are lower than that of pure Mg. The binding energies of elemental Mg in Mg-6% NiCl₂, Mg-6% CoCl₂, Mg-6% CuCl₂ and Mg-6% FeCl₃ are 49.77 eV, 49.14 eV, 49.86 eV and 48.81 eV, respectively. The lower binding energy reveals that the addition of chloride can effectively destroy the surface oxide film and leads to the explosion of non-oxide Mg, and this is consistent with the SEM images in Figure 3.

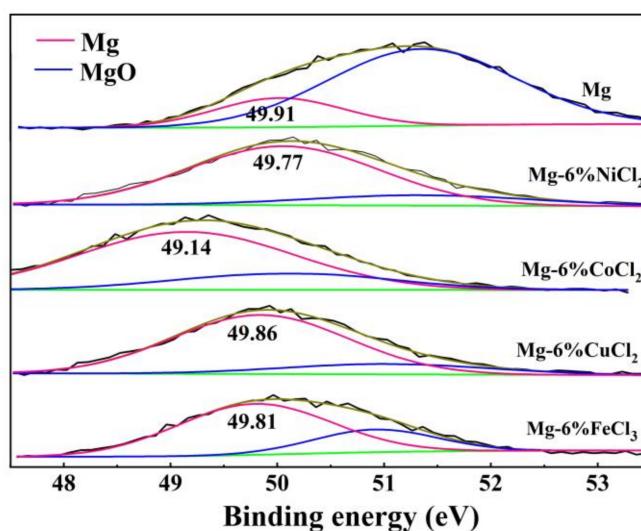


Figure 4. XPS spectra of the ball-milled Mg-chloride.

3.2. The Hydrolysis Properties of Active Mg with Different Chlorides

3.2.1. Hydrogen Generation Property

The hydrogen generation rate curves together with the temperature evolution curves during the hydrolysis processes for Mg-chloride with water were recorded as shown in Figure 5 and Table 2, respectively. The ball-milled pure Mg powders can hardly react with water, and no hydrogen is detected. The hydrogen generation curves for Mg-chloride composites show a very rapid H₂ release in the first reaction stage followed by an abrupt drop of the reaction rate as shown in Figure 5b. The rapid H₂ release durations are different for different reaction rate systems, the values change from ~50 s (for NiCl₂ composite) to ~20 s (for FeCl₃ and CuCl₂ composites). The drop of the hydrolysis reaction rate is due to the well-known formation of passive Mg(OH)₂ layer onto the Mg powder surface [20], which prevents further contact between water and unreacted Mg material and leading to low conversion yields (<80%). However, the H₂ release rate maintains a high value for all the reaction periods for the Mg-CoCl₂ composite, resulting in a better hydrolysis performance than the other Mg-chloride composites with the highest hydrogen generation conversion yield of 96.6% as shown in Table 2. The reaction temperature curves also reflect the different heat release conditions. The hydrolysis reaction of magnesium is exothermic, and the temperature change curve during the reaction can also reflect its hydrogen generation rate. High H₂ release rate can remove the generated Mg(OH)₂ on the surface and lead to the exposure of unreacted Mg, which promotes the further contact hydrolysis reaction of Mg and water.

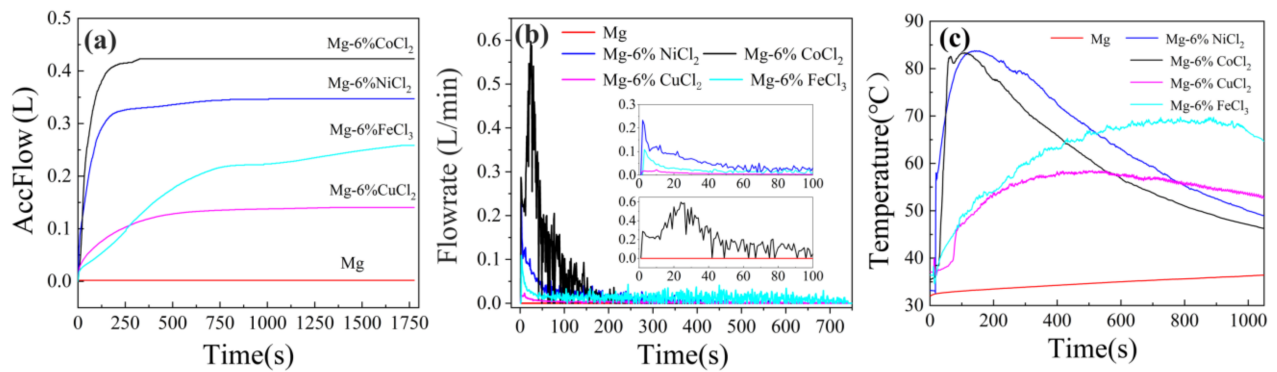


Figure 5. Hydrogen generation curves of the Mg-chloride with water (a), the hydrogen generation rate curves (b) and the temperature evolution curves (c).

Table 2. Hydrogen generation properties of ball-milled Mg-chloride with water.

| Sample (0.5 g) | Hydrogen Generation Volume (L) | Conversion Yield (%) | Maximum Hydrogen Generation Rate (L·min ⁻¹) | Reaction Duration (s) |
|------------------------|--------------------------------|----------------------|---|-----------------------|
| Mg | 0.002 | 4.28 | 0.001 | 5 |
| Mg-6%NiCl ₂ | 0.347 | 79.2 | 0.434 | 276 |
| Mg-6%CoCl ₂ | 0.423 | 96.6 | 0.597 | 325 |
| Mg-6%CuCl ₂ | 0.141 | 32.2 | 0.153 | 830 |
| Mg-6%FeCl ₃ | 0.258 | 58.9 | 0.157 | 1684 |

Note: duration refers to the time from the beginning of the reaction to the time when maximum hydrogen production is reached.

3.2.2. The Characteristics of Hydrolysis Products

The XRD patterns of the products after hydrolysis reaction of Mg-chlorides with water were illustrated in Figure 6. All products show strong peaks of Mg(OH)₂ except the ball milling Mg powder. No Mg peak can be detected in the Mg-CoCl₂ system, which indicates complete reaction for ball-milled Mg-CoCl₂.

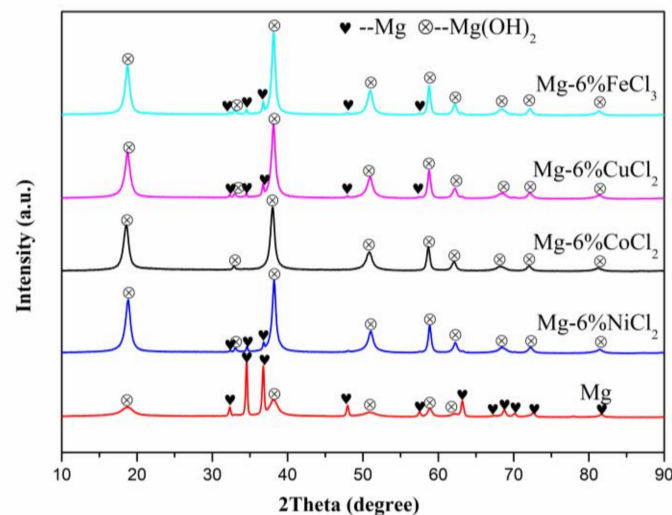


Figure 6. XRD of products after Mg-chlorides reacted with water.

The SEM images and EDS for hydrolysis reaction products of Mg-chlorides are shown in Figure 7. The Mg(OH)₂ produced by the hydrolysis reaction is in the form of nano-sized flakes but with different morphologies and sizes. The Mg(OH)₂ flakes from the production of Mg-water reaction is laid on the surface with large size, which cover the unreacted Mg surface and block the further hydrolysis reaction. However, the product exhibits separated

nano-sized particles clusters for all Mg-chlorides systems. The $\text{Mg}(\text{OH})_2$ flakes of Mg- NiCl_2 and Mg- CoCl_2 hydrolysis reaction systems have self-assembled hexagonal nanoplate morphology. Whereas, the $\text{Mg}(\text{OH})_2$ flakes present irregular aggregated plate morphology with a smaller size for products of Mg- CuCl_2 and Mg- FeCl_3 hydrolysis reaction systems. This phenomenon may be the result of thermal conditions in the reaction systems.

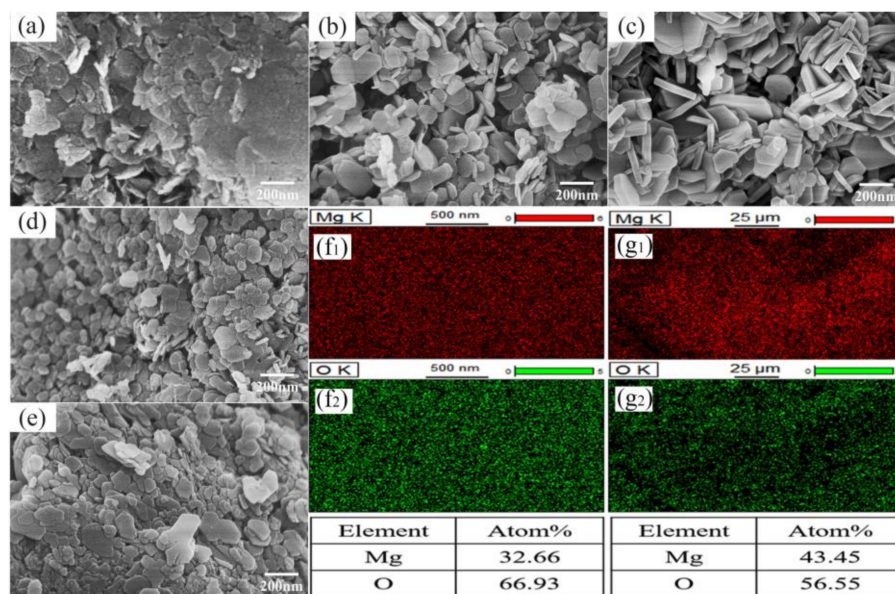


Figure 7. SEM images of products: (a) Pure Mg, (b) Mg-6% NiCl_2 , (c) Mg-6% CoCl_2 , (d) Mg-6% CuCl_2 , (e) Mg-6% FeCl_3 . (f,g) are the EDS images of (c) product of Mg-6% CoCl_2 , respectively.

The temperature curves in Figure 5c reflect the large temperature changes for Mg- NiCl_2 and Mg- CoCl_2 hydrolysis reaction systems which cause the large nucleation and growth rate, resulting in a large amount of $\text{Mg}(\text{OH})_2$ nucleation in a short time with a large growth rate. However, the new $\text{Mg}(\text{OH})_2$ nuclei always form easily on the existing ones under small thermal change conditions, and aggregated morphology forms for Mg- FeCl_3 and Mg- CuCl_2 hydrolysis reaction systems. In addition, the atomic ratio of O to Mg is studied to reveal the reaction extent. For Mg-6% CuCl_2 , the atomic ratio of O to Mg of the product is less than 2, while for Mg-6% CoCl_2 , the atomic ratio is close to 2. This indicates the existence of unreacted Mg between Mg-6% CuCl_2 and water. This phenomenon corresponds well with the XRD results in Figure 6.

4. Discussions

4.1. The Different Activation Effects of Different Chlorides

Electrochemical measurements were employed to investigate the different effects of chlorides on the reaction rate of the ball-milled Mg-chloride with water. Figure 8 shows the Tafel curves of these materials. The corrosion potential for samples of pure Mg, Mg-6% NiCl_2 , Mg-6% CoCl_2 , Mg-6% CuCl_2 and Mg-6% FeCl_3 are -0.991 V, -1.386 V, -1.596 V, -1.104 V and -1.232 V, respectively. After ball milling with chlorides, the corrosion potential of Mg in water decreases by about 0.4–0.7 V, which means that the Mg in Mg-chloride composites is hydrolyzed easier in water. Lower corrosion potential with a higher reaction rate is the result of the hydrogen generation rate shown in Figure 5b. In addition, two corrosion potentials appear in the curve of the Mg- FeCl_3 composite, which may be related to the presence of divalent and trivalent iron during the reaction.

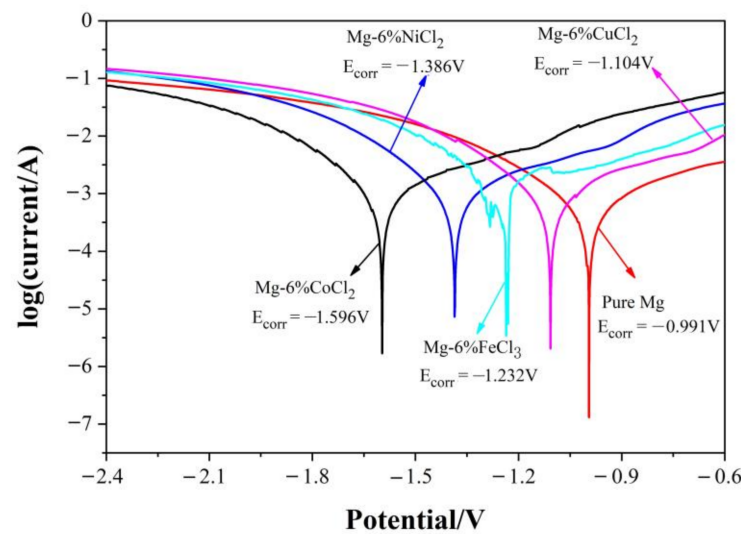


Figure 8. Tafel curves of the ball-milled Mg-chloride.

4.2. The Effects of Co on the Activation of Mg Powder

Chloride is proven to be very effective in the activation of Mg during the ball milling process. However, we cannot verify whether the effective ions are metal cations or chloride. Thus, we designed a set of comparative experiments to reveal the effect of chloride on the activation of Mg powder. Here, we take the Mg-CoCl₂ system as the investigated object for its good hydrogen generation performance. Metal Co powder was added during the ball milling process instead of chloride (6% weight percent) using the same parameters as listed in Table 1. The hydrolysis reactions were conducted in both tap water and 6% NaCl solute with the same parameters as the Mg-CoCl₂ composite. In this way, we can justify the activation mechanism in Mg-chloride composites.

The hydrogen production and hydrogen production rate are not detected by the flow meter for the reaction of Mg-6%Co with tap water. This means the reaction between Mg-6%Co and tap water is very slight. The tap water was then replaced with NaCl solution (6% in weight percent). The hydrogen production performance is shown in Figure 9a,b together with the data as listed in Table 3. The hydrogen yield of pure magnesium in NaCl solution is 0.108 L with the highest hydrogen degeneration rate of 0.132 L/min. This means that the NaCl solute is effective in enhancing the hydrolysis reaction of pure Mg. The hydrogen yield is greatly enhanced for ball milling Mg-6% Co compared with pure Mg with a higher maximum hydrogen generation rate.

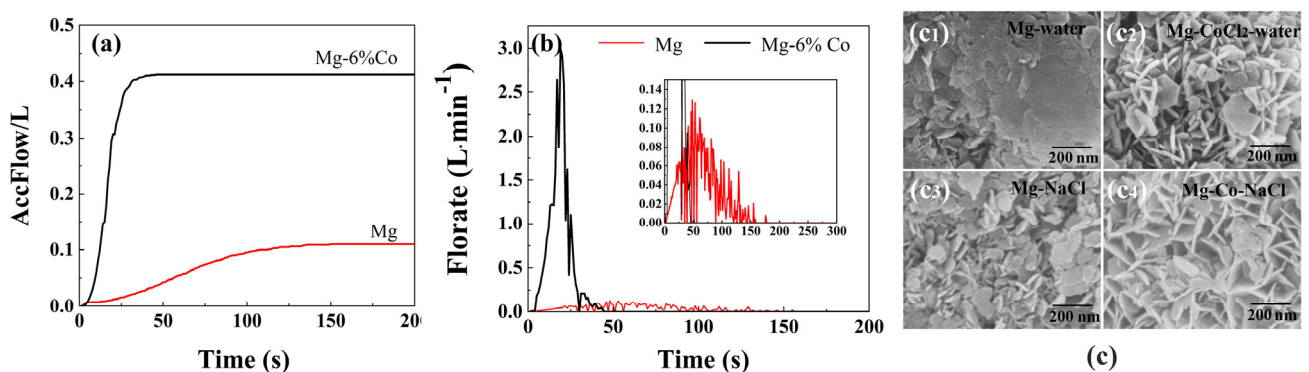


Figure 9. (a) Hydrogen generation curves of the Mg-6%Co with NaCl solute, (b) the hydrogen generation rate and (c) SEM images of reaction productions.

Table 3. Hydrogen generation properties of ball-milled Mg-6%Co with water and NaCl solute.

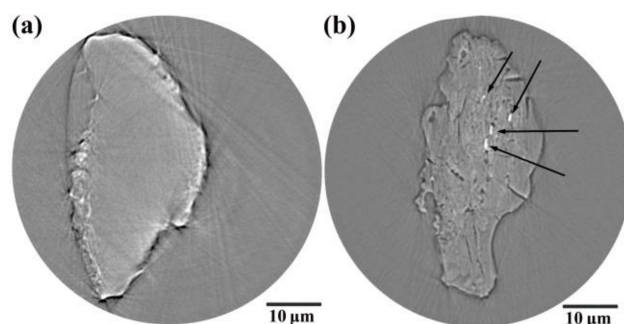
| 0.5 g | Tap Water | | | NaCl Solute | | |
|---------|-----------|----------------------|-----------------------------|-------------|----------------------|-----------------------------|
| | HGR (L) | Conversion Yield (%) | MHGR (L·min ⁻¹) | HGR (L) | Conversion Yield (%) | MHGR (L·min ⁻¹) |
| Mg | 0.000 | 0.0 | 0.000 | 0.108 | 23.1 | 0.132 |
| Mg-6%Co | 0.000 | 0.0 | 0.000 | 0.421 | 90.1 | 3.001 |

Figure 9c shows the SEM images of the hydrolysis reaction productions for different reaction systems. The morphology of Mg(OH)₂ changes from large flakes into independent self-assembled ones with the participation of NaCl for the reaction ball milling Mg with water (see Figure 9(c1,c3)). The addition of NaCl to the solute improves the crystallization behavior during the formation of Mg(OH)₂ [29] and self-assembled Mg(OH)₂ flakes fall much easier off from the Mg powder surface. In this way, more unreacted fresh Mg tends to be exposed and the hydrolysis reaction is promoted. The productions of Mg-CoCl₂-H₂O and Mg-Co-NaCl-H₂O reaction systems show similar self-assembled morphologies as seen in Figure 9(c2,c4), which means that the Co and Cl⁻ are both essential in promoting the hydrolysis reaction of Mg.

4.3. The Evolutions during Ball Milling Mg with CoCl₂

4.3.1. The Morphology Change of Mg Powder after Ball Milling with CoCl₂

Nano CT was adopted to characterize the inner microstructure of ball milling Mg and Mg-CoCl₂ powders, and Figure 10 gives the typical corresponding slice of ball milling powders (powder size < 60 μm). Spherical Mg powder changed into flakes with the thickness of 10–20 μm after ball milling for 3 h as seen in Figure 10a. No cracks exist both on the powder's surface and interior for ball milling pure Mg powder. However, numerous cracks are generated with varying sizes both on the surface and interior after ball milling with CoCl₂ for 3 h as shown in Figure 10b. These cracks are effective in exposing the fresh Mg and thus activate the hydrolysis reaction of Mg. It is interesting to see that some white particles are embedded inside the Mg flake as marked in Figure 10b. The white particles have higher density according to the phase contrast and are assumed to be Co particles in this system.

**Figure 10.** The typical slice of 3 h ball milling powders (a) Mg, (b) Mg-6%CoCl₂.

4.3.2. The Evolution of Co²⁺ during Ball Milling Mg with CoCl₂

Figure 11a shows normalized Co K-edge XANES spectra of the Mg-CoCl₂ composites as well as the reference samples of Co foil and CoCl₂. A higher valence of Co usually has an absorption edge shifting toward higher energy. Pure CoCl₂ features two peaks (A and B) of higher intensity and higher absorption edge. The XANES curves for 3 h ball-milled Mg-CoCl₂ composites powder change a lot, both in intensity and absorption edge. The absorption edge shifts toward lower photon energy, the first peak A is lower and peak B disappeared relative to the CoCl₂, as shown in Figure 10a. These changes reveal the

negative charge in comparison with the CoCl_2 , likely because Mg is an electron-donor. The obvious energy shift indicates the further electron transfer from the Mg atom to the Co^{2+} after ball milling for 3 h. The curve of Mg- CoCl_2 is more akin to Co foil, showing an intermediate state between metallic Co and CoCl_2 . Figure 11b shows the Fourier transform of the Co K-edge EXAFS oscillations in R space (phase-shift correction was not performed). The first nearest-neighbor distance for Co in Mg- CoCl_2 composite changed a lot compared with CoCl_2 , with only one single peak at the first nearest-neighbor distance being observed. This peak indicates the generation of metallic Co, which further confirms the assumption in the CT slice data (Figure 10b).

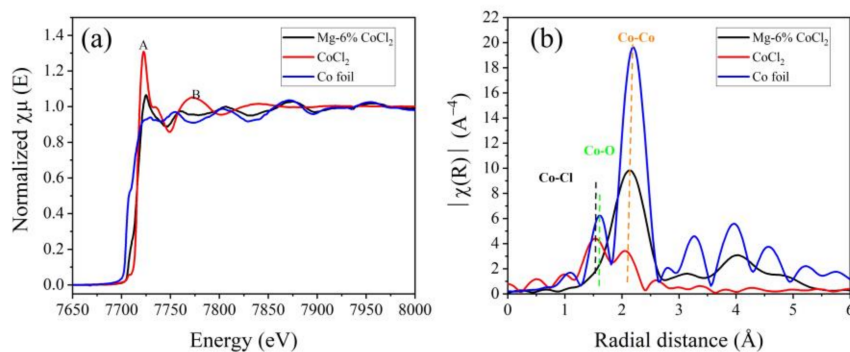


Figure 11. (a) Normalized XANES spectra at the Co K-edge, (b) Fourier-transformed extended X-ray absorption fine structure (EXAFS) of the Mg- CoCl_2 samples together with CoCl_2 and Co foil.

4.4. The Activation Mechanism

Figure 12 shows The activation mechanism. The dual existing of Co and Cl^- are essential in the activation of ball milling Mg powder as discussed in Section 4.2. For the ball milling Mg- CoCl_2 composite, the reduction reaction of cobalt ions occurs during ball milling and metallic Co generated ($\text{Co}^{2+} + \text{Mg} \rightarrow \text{Co} + \text{Mg}^{2+}$) according to the results in Sections 4.2 and 4.3. The mechanism for the activation of Mg powder promoted by chloride during ball milling can be concluded as follows:

1. Ball milling effect—The large number of cracks generated as the Mg powder with chloride is squashed and overlapped during ball milling. This leads to the exposure of fresh Mg and gives more active positions for Mg-water reaction. In addition, high potential metallics were generated as the reduction reaction occurred during ball milling promotes the corrosion of Mg.
2. The dual promoting effect of Cl^- —The existence of Cl^- in the system has two functions: one is acting as electrolyte for the Mg-M galvanic cell which accelerates the corrosion of Mg; the other is as the crystallization promoter, which modified the $\text{Mg}(\text{OH})_2$ into self-assembled morphology that easily falls off from the surface of the Mg.

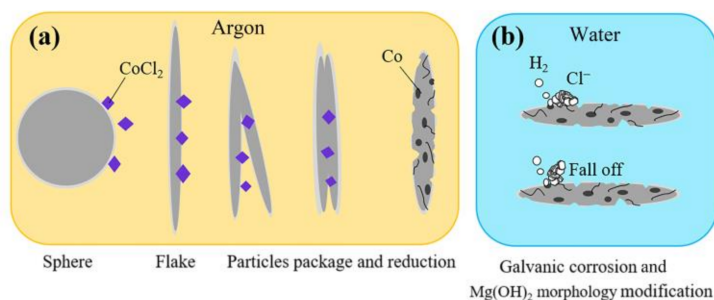


Figure 12. The activation mechanism, (a) ball milling process, (b) hydrolysis process.

5. Conclusions

In this paper, active Mg powder was prepared by ball milling with different chlorides. A much more intense and faster water reaction rate was observed after ball-milling with Mg powder and chloride compared to pure Mg. The best hydrogen performance is obtained in the Mg-6% CoCl₂ composite, which presents a high hydrolysis conversion rate of up to 96.6%, as well as a hydrogen production of 423 mL/(0.5 g). Ball milling Mg and chlorides can produce surface defects, the reduction of new high potential metallic atoms. The defects generated lead to the exposure of fresh surfaces and result in a lower binding and corrosion potential compared with pure Mg. The high potential metallic atom generated promotes the corrosion of Mg under the existence of Cl⁻. In addition, the Cl⁻ acts as the crystallization promoter, which modified the Mg(OH)₂ into a self-assembled morphology that easily falls from the surface of the Mg.

Author Contributions: Conceptualization, M.Z. and S.W.; experiments, X.W., L.Z. and X.Z.; formal analysis, S.W. and T.S.; funding acquisition, S.W.; project administration, M.Z. and S.W.; writing original draft, S.W., X.W. and X.G.; writing review and editing, S.W., X.W., M.Z. and X.L. All authors have read and agreed to the published version of the manuscript.

Funding: Postdoctoral Research Foundation of China, grant number 2019M660483.

Institutional Review Board Statement: Not applicable.

Informed Consent Statement: Not applicable.

Data Availability Statement: Data sharing not applicable.

Acknowledgments: The authors would like to thank the Postdoctoral Research Foundation of China (No. 2019M660483) for financial support; The authors also would like to thank the support given by the beamline scientist, Chunxia Yao at beamline 4W1A-X and Zhongjun Zheng at beamline 4B9A of the Beijing Synchrotron Radiation Facility (BSRF).

Conflicts of Interest: The authors declare no conflict of interest.

References

1. Bauen, A. Future energy sources and systems—Acting on climate change and energy security. *J. Power Sources* **2006**, *157*, 893–901. [[CrossRef](#)]
2. Broom, D.P.; Webb, C.J.; Hurst, K.E.; Parilla, P.A.; Gennett, T.; Brown, C.M.; Zacharia, R.; Tylianakis, E.; Klontzas, E.; Froudakis, G.E.; et al. Outlook and challenges for hydrogen storage in nanoporous materials. *Appl. Phys. A* **2016**, *122*, 151. [[CrossRef](#)]
3. Guillen, C.; Herrero, J. TCO/metal/TCO structures for energy and flexible electronics. *Thin Solid Films* **2011**, *520*, 1–17. [[CrossRef](#)]
4. Schapbach, L.; Zuttel, A. Hydrogen-storage materials for mobile applications. *Nature* **2001**, *414*, 353–358. [[CrossRef](#)] [[PubMed](#)]
5. Fan, M.Q.; Liu, S.S.; Zhang, Y.; Zhang, J.; Sun, L.-X.; Xu, F. Superior hydrogen storage properties of MgH₂-10 wt.% TiC composite. *Energy* **2010**, *35*, 3417–3421. [[CrossRef](#)]
6. Fan, M.Q.; Sun, L.-X.; Xu, F. Experiment assessment of hydrogen production from activated aluminum alloys in portable generator for fuel cell applications. *Energy* **2010**, *35*, 2922–2926. [[CrossRef](#)]
7. Kaur, M.; Pal, K. Review on hydrogen storage materials and methods from an electrochemical viewpoint. *J. Energy Storage* **2019**, *23*, 234–249. [[CrossRef](#)]
8. Fukuchi, A.; Kawashima, M.; Yuasa, S. Combustion characteristics of Mg-CO₂ counterflow diffusion flames. *Symp. Combust.* **1996**, *26*, 1945–1951. [[CrossRef](#)]
9. Shafirovich, E.Y.; Goldshleger, U.I. Combustion of magnesium particles in CO₂/CO mixtures. *Combust. Sci. Technol.* **1992**, *84*, 33–43. [[CrossRef](#)]
10. Foote, J.; Litchford, R. Powdered magnesium-carbon dioxide combustion for mars propulsion. In Proceedings of the 41st AIAA/ASME/SAE/ASEE Joint Propulsion Conference and Exhibit, Tucson, Arizona, 10–13 July 2005; p. 4469.
11. Shevtsov, V.I.; Fursov, V.P.; Stesik, L.N. Mechanism for combustion of isolated magnesium particles. *Combust. Explos. Shock. Waves* **1976**, *12*, 758–763. [[CrossRef](#)]
12. Mason, J.E. World energy analysis: H₂ now or later? *Energy Policy* **2007**, *35*, 1315–1329. [[CrossRef](#)]
13. Hou, X.; Wang, Y.; Yang, Y.; Hu, R.; Yang, G.; Feng, L.; Suo, G. Microstructure evolution and controlled hydrolytic hydrogen generation strategy of Mg-rich Mg-Ni-La ternary alloys. *Energy* **2019**, *188*, 116081. [[CrossRef](#)]
14. Xiao, F.; Guo, Y.; Yang, R.; Li, J. Hydrogen generation from hydrolysis of activated magnesium/low-melting-point metals alloys. *Int. J. Hydrog. Energy* **2019**, *44*, 1366–1373. [[CrossRef](#)]
15. Gupta, R.B. *Hydrogen Fuel: Production, Transport, and Storage*, 1st ed.; CRC Press: Boca Raton, FL, USA, 2009.

16. Macanás, J.; Soler, L.; Candela, A.M.; Muñoz, M.; Casado, J. Hydrogen generation by aluminum corrosion in aqueous alkaline solutions of inorganic promoters: The AlHidrox process. *Energy* **2011**, *36*, 2493–2501. [[CrossRef](#)]
17. Parmuzina, A.V.; Kravchenko, O.V. Activation of aluminium metal to evolve hydrogen from water. *Int. J. Hydrog. Energy* **2008**, *33*, 3073–3076. [[CrossRef](#)]
18. Kushch, S.D.; Kuyunko, N.S.; Nazarov, R.S.; Tarasov, B.P. Hydrogen-generating compositions based on magnesium. *Int. J. Hydrog. Energy* **2011**, *36*, 1321–1325. [[CrossRef](#)]
19. Grosjean, M.H.; Zidoune, M.; Roué, L. Hydrogen production from highly corroding Mg-based materials elaborated by ball milling. *J. Alloy. Compd.* **2005**, *404–406*, 712–715. [[CrossRef](#)]
20. Grosjean, M.H.; Zidoune, M.; Roué, L.; Huot, J.Y. Hydrogen production via hydrolysis reaction from ball-milled Mg-based materials. *Int. J. Hydrog. Energy* **2006**, *31*, 109–119. [[CrossRef](#)]
21. Huang, M.; Ouyang, L.; Ye, J.; Liu, J.; Yao, X.; Wang, H.; Shao, H.; Zhu, M. Hydrogen generation via hydrolysis of magnesium with seawater using Mo, MoO₂, MoO₃ and MoS₂ as catalysts. *J. Mater. Chem. A* **2017**, *5*, 8566–8575. [[CrossRef](#)]
22. Huang, H.T.; Zou, M.S.; Guo, X.Y.; Yang, R.J.; Li, Y.K. Study of reactions of activated Mg-based powders in heated steam. *J. Power Sources* **2014**, *246*, 960–964. [[CrossRef](#)]
23. Zou, M.; Guo, X.; Huang, H. Preparation and characterization of hydro-reactive Mg–Al mechanical alloy materials for hydrogen production in seawater. *J. Power Sources* **2012**, *219*, 60–64. [[CrossRef](#)]
24. Matsuzaki, K.; Murakami, T. Formation of Hydrogen by Ball Milling of Mg and Mg Alloy in Seawater. *Mater. Sci. Forum* **2017**, *879*, 1265–1269. [[CrossRef](#)]
25. Kravchenko, O.V.; Sevastyanova, L.G.; Urvanov, S.A.; Bulychev, B.M. Formation of hydrogen from oxidation of Mg, Mg alloys and mixture with Ni, Co, Cu and Fe in aqueous salt solutions. *Int. J. Hydrog. Energy* **2014**, *39*, 5522–5527. [[CrossRef](#)]
26. Liu, Y.; Wang, X.; Dong, Z.; Liu, H.; Li, S.; Ge, H.; Yan, M. Hydrogen generation from the hydrolysis of Mg powder ball-milled with AlCl₃. *Energy* **2013**, *53*, 147–152. [[CrossRef](#)]
27. Wang, X.; Zhang, Q.; Shi, X.; Wang, N.; Chai, Y. Synergistic effect of the fresh Co, Ni, and anion ions on aluminum or magnesium with water reactions. *Int. J. Energy Res.* **2019**, *43*, 430–438. [[CrossRef](#)]
28. Sun, Q.; Zou, M.; Guo, X.; Yang, R.; Huang, H.; Huang, P.; He, X. A study of hydrogen generation by reaction of an activated Mg–CoCl₂ (magnesium–cobalt chloride) composite with pure water for portable applications. *Energy* **2015**, *79*, 310–314. [[CrossRef](#)]
29. Song, X.; Sun, S.; Zhang, D.; Wang, J.; Yu, J. Synthesis and characterization of magnesium hydroxide by batch reaction crystallization. *Front. Chem. Sci. Eng.* **2011**, *5*, 416–421. [[CrossRef](#)]